A minimally disruptive method for measuring water potential in planta using hydrogel nanoreporters

Piyush Jain[a,1], Weizhen Liu[b,1,2], Siyu Zhu[c], Christine Yao-Yun Chang[d], Jeff Melkonian[d], Fulton E. Rockwell[e], Duke Pauli[b,3], Ying Sun[d], Warren R. Zipfel[f], N. Michele Holbrook[e], Susan Jean Riha[g], Michael A. Gore[b], and Abraham D. Stroock[c,h,4]

[a]Sibley School of Mechanical and Aerospace Engineering, Cornell University, Ithaca, NY 14853; [b]Plant Breeding and Genetics Section, School of Integrative Plant Science, Cornell University, Ithaca, NY 14853; [c]Smith School of Chemical and Biomolecular Engineering, Cornell University, Ithaca, NY 14853; [d]Soil and Crop Sciences Section, School of Integrative Plant Science, Cornell University, Ithaca, NY 14853; [e]Department of Organismic and Evolutionary Biology, Harvard University, Cambridge, MA 02138; [f]Department of Biomedical Engineering, Cornell University, Ithaca, NY 14853; [g]Department of Earth and Atmospheric Sciences, Cornell University, Ithaca, NY 14853; and [h]Kavli Institute at Cornell for Nanoscale Science, Cornell University, Ithaca, NY 14853

Edited by Julian I. Schroeder, University of California San Diego, La Jolla, CA, and approved April 7, 2021 (received for review May 29, 2020)

Leaf water potential is a critical indicator of plant water status, integrating soil moisture status, plant physiology, and environmental conditions. There are few tools for measuring plant water status (water potential) in situ, presenting a critical barrier for developing appropriate phenotyping (measurement) methods for crop development and modeling efforts aimed at understanding water transport in plants. Here, we present the development of an in situ, minimally disruptive hydrogel nanoreporter (AquaDust) for measuring leaf water potential. The gel matrix responds to changes in water potential in its local environment by swelling; the distance between covalently linked dyes changes with the reconfiguration of the polymer, leading to changes in the emission spectrum via Förster Resonance Energy Transfer (FRET). Upon infiltration into leaves, the nanoparticles localize within the apoplastic space in the mesophyll; they do not enter the cytoplasm or the xylem. We characterize the physical basis for AquaDust's response and demonstrate its function in intact maize (*Zea mays* L.) leaves as a reporter of leaf water potential. We use AquaDust to measure gradients of water potential along intact, actively transpiring leaves as a function of water status; the localized nature of the reporters allows us to define a hydraulic model that distinguishes resistances inside and outside the xylem. We also present field measurements with AquaDust through a full diurnal cycle to confirm the robustness of the technique and of our model. We conclude that AquaDust offers potential opportunities for high-throughput field measurements and spatially resolved studies of water relations within plant tissues.

responsive hydrogel | nanobiosensors | water potential | plant–water relations

Plant life depends on water availability. In managing this demand, irrigated agriculture accounts for 70% of all human water use (1). Physiologically, the process of transpiration (E) dominates this demand for water (Fig. 1*A*): Solar thermal radiation and the unsaturated relative humidity in the atmosphere drive evaporation from the wet internal surfaces of leaves; this water loss pulls water up through the plant's vascular tissue (xylem) and out of the soil. This flow occurs along a gradient in the chemical potential of water, or water potential, ψ [MPa] (2). Studies of water relations and stress physiology over the past decades have found that values of ψ along the path of E (the soil–plant–atmosphere continuum [SPAC]) correlate with plant growth, crop yield and quality, susceptibility to disease, and the balance between water loss due to E and the uptake and assimilation of carbon dioxide (water-use efficiency) (3–5).

Due to the recognized importance of water potential in controlling plant function, plant scientists have spent considerable effort devising accurate and reliable methods to measure water potential of the soil, stem, and leaf (6). Of these, plant water potentials, and particularly leaf water potential (ψ^{leaf}), represent valuable indicators of plant water status because they integrate both environmental conditions (e.g., soil water availability and evaporative demand) and plant physiological processes (e.g., root water uptake, xylem transport, and stomatal regulation) (7, 8). To date, techniques to measure ψ^{leaf} remain either slow, destructive, or indirect. The current tools (e.g., Scholander pressure chamber, psychrometer, and pressure probe) involve disruption of the tissue, the microenvironment, or both (9–11). For example, the widely used pressure chamber requires excision of leaves or stems for the measurement of ψ^{leaf}. Other techniques, such as stem and leaf psychrometry, require intimate contact with the tissue, and accurate and repeatable measurements are difficult to obtain (9, 12). These limitations have

Significance

Gaps in our ability to document local water relations in leaves compromise our ability to build complete models of leaf and plant function and our understanding of ecophysiological phenomena, such as response and adaptation to drought. Macroscopically, leaf water potential has been shown to impact vegetative growth and yield, susceptibility to disease, and, in extreme drought, plant viability, making it a promising candidate trait to improve water-use efficiency in plants. In this paper, we present a nanoscale sensor (AquaDust) that provides minimally disruptive measurements of water potential in leaves of intact plants at high spatial and temporal resolution. This creates opportunities for improving our understanding of the mechanisms coupling variations in water potential to biological and physical processes.

Author contributions: P.J., W.L., C.Y.-Y.C., J.M., F.E.R., D.P., Y.S., W.R.Z., N.M.H., S.J.R., M.A.G. and A.D.S. designed research; P.J., W.L., S.Z., C.Y.-Y.C. and F.E.R. performed research; P.J., W.L., S.Z., J.M., S.J.R., M.A.G. and A.D.S analyzed data; and P.J., W.L., J.M., S.J.R., M.A.G. and A.D.S. wrote the paper.

Competing interest statement: P.J., D.P., M.A.G., and A.D.S. are listed as inventors on a patent application (International Publication No. WO2019023712A1) titled "In Situ Sensing of Water Potential" filed by Cornell University.

This article is a PNAS Direct Submission.

[1]P.J. and W.L. contributed equally to this work.

[2]Present address: School of Computer Science and Technology, Wuhan University of Technology, Wuhan 430070, China.

[3]Present address: School of Plant Sciences, University of Arizona, Tucson, AZ 85721.

[4]To whom correspondence may be addressed. Email: abe.stroock@cornell.edu.

This article contains supporting information online at https://www.pnas.org/lookup/suppl/doi:10.1073/pnas.2008276118/-/DCSupplemental.

Published May 31, 2021.

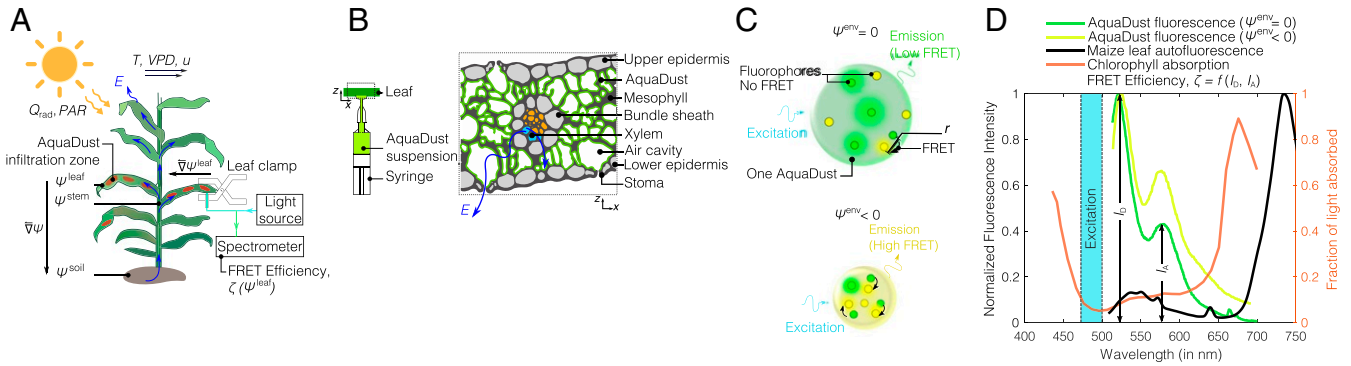

Fig. 1. AquaDust as an in situ reporter of water potential (ψ). (*A*) Schematic representation of a maize plant undergoing transpiration (*E*) in a dynamic environment driven by solar thermal radiation (Q_{rad}) and photosynthetically active radiation (*PAR*), wind speed (*u*), temperature (*T*), vapor pressure deficit (*VPD*), and soil water potential (ψ^{soil}). Water flows through the plant (blue arrows) along a gradient in water potential ($\vec{\nabla}\psi$). Zones on the leaves infiltrated with AquaDust serve as reporters of the local leaf water potential, ψ^{leaf}, via a short ($\sim$ 30 s), minimally invasive measurement of FRET efficiency (ζ) with a leaf clamp. (*B*) Schematic representations of infiltration of a suspension of AquaDust and of the distribution of AquaDust within the cross-section of a leaf. AquaDust passes through the stomata and localizes in the apoplastic spaces within the mesophyll; the particles are excluded from symplastic spaces and the vascular bundle. (*C*) Schematic diagrams showing mechanism of AquaDust response: The swollen, "wet" state when water potential in its local environment, $\psi^{env} = 0$ (i.e., no stress condition), results in low FRET between donor (green circles) and acceptor (yellow circles) dye (*Upper*); and the shrunken, "dry" state when $\psi^{env} < 0$ (i.e., stressed condition) results in high FRET between fluorophores, thereby altering the emission spectra (*Lower*). (*D*) Fluorescent dyes were chosen to minimize reabsorption of AquaDust emission from chlorophyll; comparison of representative fluorescent emission from AquaDust (donor peak at 520 nm and acceptor peak at 580 nm) with the absorption spectra of chlorophyll and autofluorescence of maize leaf.

hindered the study of spatiotemporal water-potential gradients along the SPAC and the development of high-throughput strategies to phenotype based on tissue water potential (13). Additionally, current methods for measuring ψ^{leaf} provide averages over tissues in the leaf. This characteristic makes the dissection of water relations on subleaf scales challenging, such that important questions remain, for example, about the partitioning of hydraulic resistances within leaves between the xylem and mesophyll (14–16).

These outstanding challenges in the measurement of water status in planta motivated us to develop the measurement strategy presented here, AquaDust, with the following characteristics: 1) Minimally disruptive: Compatible with simple, rapid measurements on intact leaves. Fig. 1*A* presents our approach, in which AquaDust reporters infiltrated into the mesophyll of the leaf provide an externally accessible optical signal that correlates with the local water potential. 2) Localized: allowing for access to the values of water potential at a well-defined location along the path of transpiration in the leaf tissue. Fig. 1*B* shows a schematic representation of AquaDust particles localized in the apoplastic volume within the mesophyll, at the end of the hydraulic path for liquid water within the plant. 3) Sensitive and specific: capable of resolving water potentials across the physiologically relevant range ($\sim -3 < \psi < 0$ MPa) and with minimal sensitivity to other physical (e.g., temperature) and chemical (e.g., pH) variables. Fig. 1*C* presents a schematic representation of an AquaDust particle formed of hydrogel, a highly tunable material that undergoes a structural response to changes in local water potential (swollen when wet; collapsed when dry). We couple the swelling behavior of the particle to an optical signal via the incorporation of fluorescence dyes (green and yellow circles in Fig. 1*C*) that undergo variable Förster Resonance Energy Transfer (FRET) as a function of spatial separation. Fig. 1*D* presents typical AquaDust spectra at high (wet; green curve) and low (dry; yellow curve) water potentials. A change in water potential leads to a change in the relative intensity of the two peaks in the AquaDust spectrum, such that the relative FRET efficiency, $\zeta = f(I_D, I_A)$, can serve as a measure of water potential. 4) Inert: nondisruptive of the physiological properties of the leaf (e.g., photosynthetic capacity, transpiration rate, etc.).

In this paper, we present the development, characterization, and application of AquaDust. We show that AquaDust provides a robust, reproducible response of its fluorescence spectra to changes in leaf water potential in situ and across the usual physiological range. We apply our approach to quantify the spatial gradients of water potential along individual leaves undergoing active transpiration and across a range of soil water potentials. With these measurements, we show that the localization of AquaDust in the mesophyll allows us to quantify the importance of hydraulic resistances outside the xylem. We further use AquaDust to measure the diurnal dynamics of ψ^{leaf} under field conditions, with repeated measurements on individual, intact leaves. These measurements demonstrate the field-readiness of our techniques and validate the leaf hydraulic model we have developed. We conclude that AquaDust offers a powerful basis for tracking, spatially and temporally, water potential in planta to study the mechanisms by which it couples to both biological and physical processes to define plant function.

Results and Discussion

AquaDust Design and Synthesis. We provide a detailed explanation of the design and synthesis of AquaDust in *SI Appendix* (sections S1–S4). Here, we briefly discuss our considerations in designing these reporters. In the selection of a specific hydrogel matrix, we used literature, theory, and experimentation to guide our design: We selected poly(acrylamide), a neutral polymer with weakly temperature-dependent swelling (17, 18), to minimize dependence on pH, ionic strength, and temperature; and we followed Flory–Rehner theory to tune the polymer fraction (*SI Appendix*, section S2A; refs. 19–24) with the estimate of the chemical affinity of the polymer for water (i.e., the Flory–Chi parameter, χ), as obtained from the swelling behavior of macroscopic gels (*SI Appendix*, section S3 and Table S1), to match the range of the swelling transition to the physiological range of water potential ($0 > \psi > -3$ [MPa]). In the selection of specific dyes for the FRET response, we chose fluorophores for which the peaks of excitation and emission fall between the peaks of absorption of chlorophyll and can be distinguished from the peak in chlorophyll autofluorescence (Fig. 1*D*). We used Flory–Rehner theory and a dipole-plane FRET model to iteratively

find an optimal combination of monomer and cross-linker concentration, with fixed dye concentration, to maximize ζ in the range of $0 > \psi > -3$ [MPa] (*SI Appendix*, section S2 A–C and Fig. S1) (25–28). Importantly, we found that a combined theory based on Flory–Rehner swelling and dipole-plane FRET interactions allowed us to describe the calibration function, $\zeta(\psi)$, with a single adjustable parameter (the effective interdye separation in the swollen state) (*SI Appendix*, sections S2D and S3 and Figs. S2 and S3). The robustness of this theory allows us to calibrate AquaDust at a single point (e.g., saturation) in situ.

In defining the size of AquaDust particles, the need to deliver them through the stomata and to minimize obstruction of internal cavities within the mesophyll set a micrometer-scale upper bound; the need to accommodate FRET pairs with separations ranging from 4 to 10 nm and avoid passage through the pores of cell walls set a lower bound of ~ 10 nm [it is reported that the nanoparticles less than 10 nm in diameter can translocate through the cell-wall pores (29)]. To achieve size control, we synthesized hydrogel nanoparticles using inverse microemulsion polymerization with acrylamide as the monomer and *N*-aminopropyl methacrylamide as a primary amine-bearing comonomer for reaction with donor and acceptor fluorophores conjugated via *N*-hydroxysuccinimidyl ester (30–33) (see *SI Appendix*, section S4 A and B and Fig. S4 for details on AquaDust synthesis). We chose an appropriate water-to-oil ratio and surfactant concentration to regulate the size of the aqueous core of the reverse micellar droplets (34). After synthesis, the size of these nanoparticles was 42 nm (number-averaged mean) with an SD of 13 nm, as measured by using the dynamic light-scattering technique (*SI Appendix*, section S4C and Fig. S5).

AquaDust Characterization and Localization. We used maize (*Zea mays* L.) as the model species for characterization of AquaDust. Maize is one of the three most important cereal crops for world food security; knowledge of its water-stress physiology is key to improving drought tolerance (35–37). We infiltrated AquaDust in the maize leaves by injecting the suspension with pressure through the stomata on the abaxial surface of the intact leaf (Fig. 1*B*). We used AquaDust concentration of 6.6×10^8 particles per mL with deionized water as solvent. We selected this concentration such that AquaDust fluorescent intensity was 10-fold higher than the chlorophyll autofluorescence, ensuring high signal-to-background intensity. We used deionized water as the suspension medium to minimize particle aggregation prior to infiltration (see *SI Appendix*, section S4C for details).

Immediately after the infiltration, the zone into which the suspension permeated appeared dark (Fig. 2*A*). In maize, this zone typically extended ~ 6 mm laterally and ~ 40 mm axially from the point of injection; the asymmetry of this spreading is expected, given the axial connectivity of vapor spaces in the mesophyll of maize leaves (38). We allowed the infiltrated suspension to come to equilibrium in the leaf under standard growing conditions for 24 h before measurement of water potential; after this equilibration, the appearance of the infiltrated zone returned to that of the surrounding, noninfiltrated tissue. We used gas-exchange measurements to define this waiting time: 24 h after infiltration, we observed no significant difference between the physiological parameters such as CO_2 and water-vapor exchange rates between areas of maize leaves with and without infiltration of AquaDust, as discussed below (also see *SI Appendix*, section S4E and Table S2). At the site of infiltration, we typically observed some mechanical disturbance of the cuticle. We avoided interrogating AquaDust at this spot, also discussed below.

Fig. 2*B* shows the autofluorescence from the bundle sheath cells and mesophyll cells (false-colored as blue), as acquired by confocal fluorescence microscopy (see *SI Appendix*, section S4D for details). In the top-view micrograph of the leaf without AquaDust, the autofluorescence false-colored as blue denotes the mesophyll and bundle sheath cells (39) (see *SI Appendix*, section S4D for details on sample preparation and *SI Appendix*, Fig. S6 for cross-section view). In the top-view micrograph of an intact leaf infiltrated with AquaDust, the excitation of AquaDust resulted in fluorescence false-colored as yellow (Fig. 2*C*). We see that AquaDust colocated with the cell walls, predominantly in areas exposed to vapor pockets within the mesophyll, as seen in the micrograph in Fig. 2*B*. This distribution suggests that the AquaDust particles mostly coat, rather than penetrate, the cell wall. We do see some evidence of penetration into nonexposed apoplastic spaces (e.g., between adjacent cells), despite the expectation that the particles >10 nm in diameter should be excluded from passage through cell walls (29). It is possible that some permeation of the nanoporous cell wall may occur due to the soft nature of the gel particles. Fig. 2*C* clearly shows that the AquaDust was excluded from the cytosol of all cells (mesophyll, epidermal, and bundle sheath cells) and from the vascular bundles. Images of full cross-sections show that this localization pattern continues through the full section of the leaf (see *SI Appendix*, Fig. S6 for the cross-section view of leaf with and without AquaDust). Importantly, the localization of AquaDust within the apoplast places it at the end of the transpiration path, providing an unprecedented opportunity to probe the thermodynamic state of water near the sites of gas exchange with the atmosphere.

To assess the effect of AquaDust infiltration on the physiological function of leaves, we compared the CO_2 and water-vapor exchange rates between areas of maize leaves with and without infiltration of AquaDust. We observed no significant impact of AquaDust on leaf physiological parameters (transpiration rate, assimilation rate, and stomatal conductance; *SI Appendix*, section S4E and Table S2).

In Planta Measurements and Calibration. In order to perform minimally invasive interrogations of the state of AquaDust within the leaf tissue, we developed the platform illustrated in Fig. 3*A*: We used an excitation source (mercury halide light source), appropriate excitation and collection filters, optical fiber probes, a leaf clamp designed to block the ambient light and to position the reflection probe (the leaf clamp did not bring the optical assembly into direct contact with the leaf), and a spectrometer to collect the fluorescence emission spectra (see details in *SI Appendix*, section S4F and Fig. S7). A typical measurement involved clamping the leaf for a duration of less than 30 s. Fig. 3*B* shows the emission spectra from AquaDust on intact maize leaves as we subjected the potted plants to dry-down in order to progressively reduce ψ^{leaf} (for details, see *SI Appendix*, section S4G). We observed obvious, qualitative changes in the fluorescence spectrum from the leaf: The relative intensity of the acceptor dye at ~ 580 nm rose significantly with decreasing ψ^{leaf}, as measured using a pressure chamber ($\psi^{\text{leaf}}_{\text{PC}}$; see *SI Appendix*, section S4G for details on how the pressure-chamber measurement was performed). Importantly, this large change in intensity occurred over a range of ψ^{leaf} typically encountered during plant water stress for most agriculturally relevant species, including maize (0 to -1.5 MPa) (40). We verified that there was minimal variation in absorbance spectra of the leaf (indirect measure of concentration of pigments such as chlorophyll, anthocyanins, etc.), suggesting that the AquaDust response is minimally affected by variation in chemical concentration of pigments, in this range of ψ^{leaf} (see *SI Appendix*, section S4H and Fig. S8 for details).

The spectra in Fig. 3*B* allowed us to calibrate the AquaDust response relative to pressure-chamber measurements of ψ^{leaf}. From AquaDust emission spectra (Fig. 3*B*), we

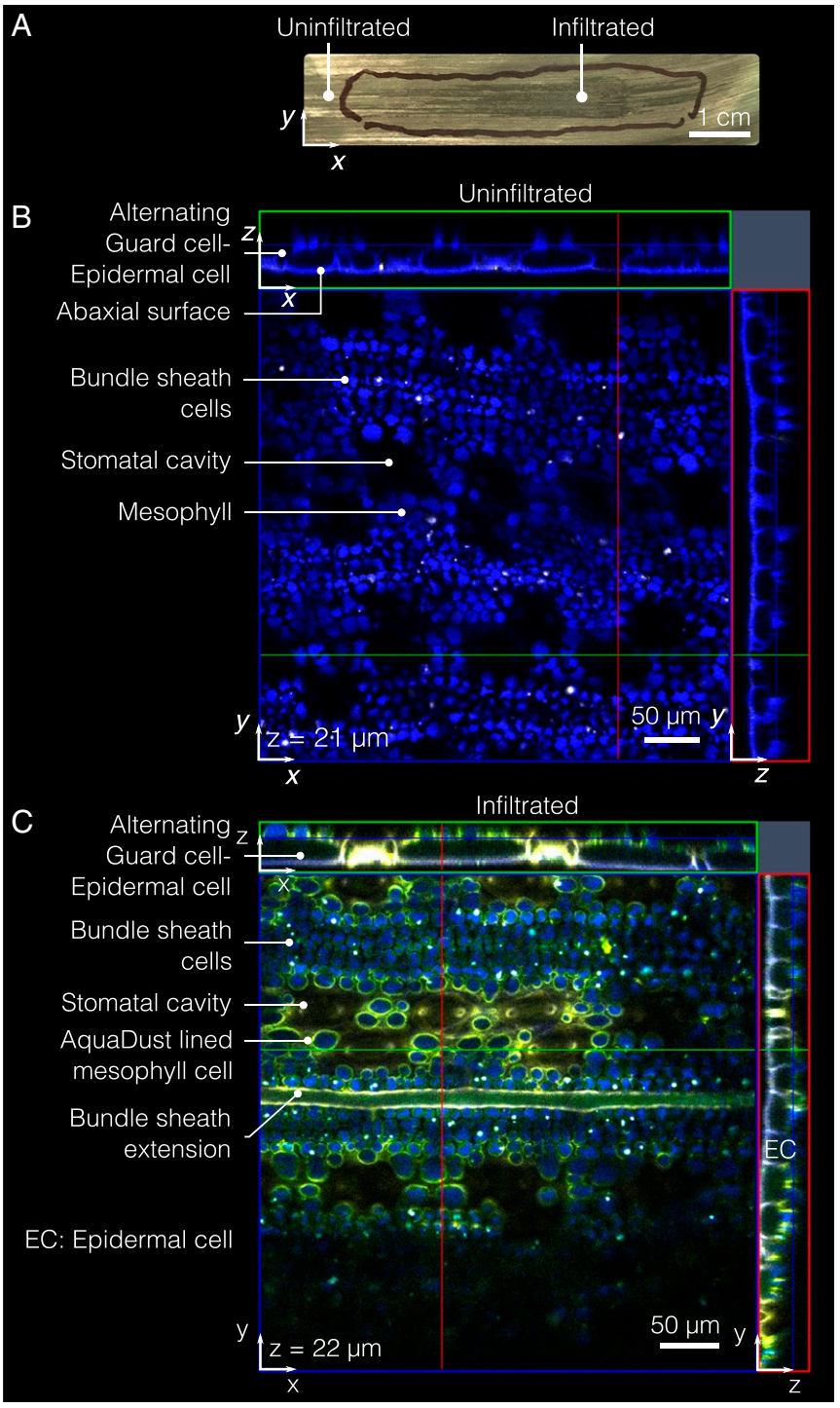

Fig. 2. AquaDust distribution within mesophyll. (*A*) Typical infiltration of AquaDust suspension in maize leaf is evident with darkening of infiltrated zone immediately after infiltration; the discoloration dissipates within ~2 h as the injected zone re-equilibrates with the surrounding tissue. (Scale bar: 1 cm.) (*B*) Cytosol and cuticle autofluorescence (blue) from an uninfiltrated maize leaf imaged from the abaxial side using confocal microscope with *xz*- and *yz*-planes at locations denoted by green and red lines. (*C*) Cytosol and cuticle autofluorescence (blue) and AquaDust fluorescence (yellow) as seen from the abaxial side of maize leaf under confocal microscope infiltrated with AquaDust suspension. (See *SI Appendix*, section S4D for details of preparation and imaging.)

extracted experimental values of relative FRET efficiency, ζ_{exp}, as a function of the ratio of intensity of the acceptor peak (~580 nm) to that of the donor peak (~520 nm) (Fig. 1*D*; *SI Appendix*, section. S3B.1). In Fig. 3*C*, we plot ζ_{exp} from the emission spectra (Fig. 3*B*) against the $\psi_{\mathrm{PC}}^{\mathrm{leaf}}$ (see *SI Appendix*, Table S3 for the numerical values). The measured values of FRET efficiencies fit a first-principles model (dashed curve) that couples the hydrogel swelling as a function of water potential (Flory–Rehner) and the FRET interaction [dipole-plane interaction (41–46); for details on comparison with other models (47), see *SI Appendix*, section S2 B and D and Fig. S2]. As with the ex situ calibration (*SI Appendix*, Fig. S3), this in situ calibration involved adjusting a

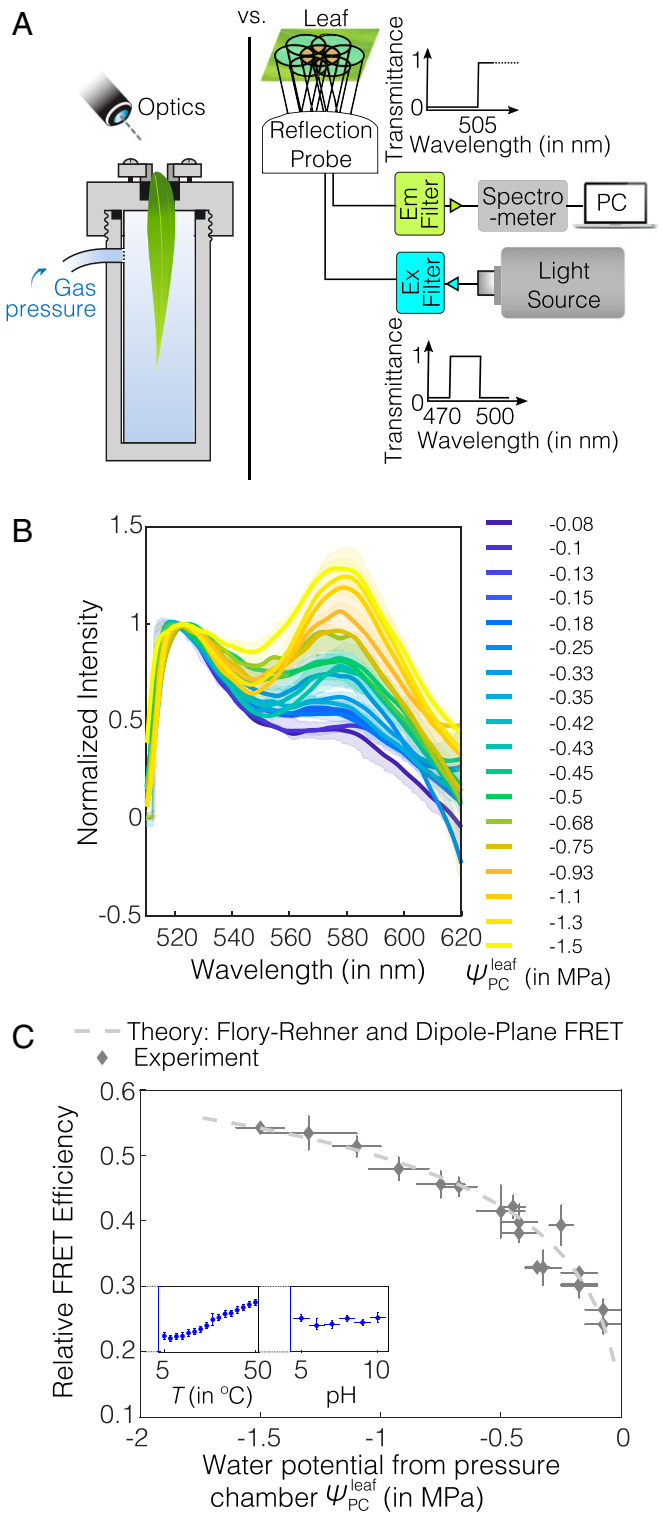

Fig. 3. AquaDust response to leaf water potential. (*A*) Schematic diagrams shows calibration against Scholander pressure chamber (*Left*) and instrumentation for a typical in situ measurement (*Right*): A mercury lamp was used as source for illumination, and a narrow-band-wavelength optical filter was used to select the excitation-light wavelength (here, it is 470 to 500 nm) used to excite AquaDust using a reflection probe. The reflected light was captured by the central fiber and sent to the spectrometer after filtering out the reflected excitation wavelengths using an emission filter to avoid the saturation of detector; spectrometer output was recorded and saved. (*B*) Spectra of AquaDust in maize leaves at different water potentials as measured with a pressure chamber, ψ_{PC}^{leaf}, on the tip of actively transpiring maize leaves. Bold lines represent spectra closest to the mean FRET efficiency, and the translucent band represents the error in the spectra, as obtained from three to six measurements. The legend provides mean values of ψ_{PC}^{leaf} corresponding to each spectrum. (*C*) Relative FRET efficiency as calculated from the spectra in *B* is plotted against ψ_{PC}^{leaf}. A theoretical prediction as obtained from the Flory–Rehner theory and dipole-plane FRET model is plotted against water potential. (See *SI Appendix*, Table S3 for the numerical values of the plotted data.) The vertical error bars represent the range of relative FRET efficiency from AquaDust, and the horizontal error bars represent the range of water potential from pressure chamber. *C*, *Inset* shows the response in terms of the relative FRET efficiency of AquaDust suspension (*y* axis ranges from 0.2 to 0.3) to temperature ranging from 5 to 50°C and pH of the buffer ranging from 5 to 10 (see *SI Appendix*, section S4 M and N for details).

single parameter, c (separation of dyes at saturation); by fitting the theoretical FRET efficiency to the experimental FRET efficiency ($\zeta_{th} = \zeta_{exp}$) at a single measurement point (here, closest to saturation: $\psi_{PC}^{leaf} = -0.08$ MPa), we can accurately represent the response across the full range. The requirement of a single calibration measurement limits the time required to initiate use of each new batch of AquaDust as a sensor for measuring water potential. This robust, simple behavior was reproducible across the plants we have investigated (including other species such as coffee [*Coffea arabica* L.] and Phytolacca [*Phytolacca Americana* L.]; see *SI Appendix*, section S4I and Fig. S9 for details) and was stable for at least 5 d in fully illuminated conditions in the greenhouse (see *SI Appendix*, section S4I for greenhouse conditions). The experimental FRET efficiency calculated by using fluorescence spectra could potentially have artifacts arising from differential bleaching of fluorophores and errors arising from cross-excitation (48). We compared the relative FRET efficiency calculated by using spectra with the relative FRET efficiency calculated by using lifetime imaging, and we found no significant difference ($P > 0.05$) between the relative FRET efficiency calculated from these two different techniques (*SI Appendix*, section S4J, Fig. S10, and Table S4).

Averaged over all of the readings, the difference between mean value of ψ_{AQD}^{leaf} and the mean value of ψ_{PC}^{leaf} was 0.018 MPa with an SD of 0.067 MPa (for in vitro measurements, mean error was 0.02 MPa and SD was 0.06 MPa, similar as for the in planta measurements; see *SI Appendix*, section S2D and Fig. S3 for details). Based on the uncertainty associated with the experimental value of ψ_{PC}^{leaf} and multiple measurements from AquaDust, we found that the uncertainty in ψ_{AQD}^{leaf} was ± 0.14 MPa based on the 95% CI estimate for the model, compared with ± 0.05 MPa for the Scholander pressure chamber (see *SI Appendix*, section S4K and Fig. S11 for analysis). This uncertainty is sufficiently small for most studies of water relations, given that the range of ψ^{leaf} typically encountered during plant water stress is 0 to -1.5 MPa (49).

As noted before, we observed mechanical damage on the cuticle during injection of AquaDust by pressure infiltration (Fig. 2*A*); this could result in AquaDust around the site of injection being exposed to the external vapor environment. We found that the water-potential reading from AquaDust was uniform and stable when acquired at a distance of more than 3 mm away from the site of infiltration (*SI Appendix*, section S4L and Fig. S12). We observed no specific trend in AquaDust measurements with increasing distance from the site of infiltration. As a result, all measurements from AquaDust were taken >1 cm away from the site of infiltration to ensure reliable measurements of ψ^{leaf}. Since the extent of AquaDust infiltration extends $\gtrsim 4$ cm from the site of infiltration in maize (Fig. 2*A*), the effect of damage due to injection could be reasonably avoided.

In order to deploy AquaDust in living plant tissues as a reporter of water potential, it is crucial to characterize AquaDust

response to other physical and chemical variables, such as temperature and pH. As shown in Fig. 3*C*, *Inset*, we found small changes (within the uncertainty range of water potential measured using AquaDust, i.e., ±0.14 MPa) in AquaDust FRET efficiency over a relatively broad temperature range ($\sim 5-50^{\circ}$C) (see *SI Appendix*, section S4M and Fig. S13 for details) (50). This observation is consistent with the reported studies that the change in swelling of acrylamide gel in response to temperature is negligible (17, 18). Also, the AquaDust response was relatively insensitive (within the uncertainty range of water potential measured using AquaDust, as described in next section, ±0.14 MPa) over a pH range of 5 to 10 (51) because of the use of nonionic, unhydrolyzed polyacrylamide gels in the synthesis of AquaDust (*SI Appendix*, section S4N and Fig. S14) (52–54).

Water-Potential Gradients along the Leaf. AquaDust opens a route to investigate local water potentials to understand and model water-potential gradients in plants. As an example, we used AquaDust to track changes in ψ along a leaf blade to characterize key resistances to water flow in leaves.

Water moves axially from the node through the xylem and laterally from the xylem into the surrounding mesophyll, down gradients in water potential resulting from the flux of water out of the surfaces of the leaf. These gradients within leaves and the resistances that control them have remained difficult to characterize, despite the roles they have been suggested to play in stomatal regulation of gas exchange (55) and in nonstomatal regulation of water status (56). The whole-leaf hydraulic resistance has often been measured by recording the changes in the flux of water in excised leaves with varying degrees of water stress (ψ^{leaf}) (57). Recent experimental studies involving quantitative measurements of leaf-xylem conductance (58, 59) and models of leaf-xylem and outside-xylem conductance (60, 61) have distinguished the resistances of the xylem and the outside-xylem components of the pathway and the distinct dependencies of these resistances on average leaf water potential; these studies suggest that the outside-xylem resistance can contribute greater than 75% of the total leaf resistance upon dehydration. However, these experimental studies have relied on excised plant material and vein cutting (vacuum-chamber method) to distinguish the relative contributions of xylem embolism and changes in outside-xylem properties to explain the whole-leaf hydraulic decline (58, 59). Significant uncertainty remains in the interpretation of these resistances in terms of local physiology [e.g., embolism (62) or deformation of the xylem (63) and changes in aquaporin-mediated conductance outside the xylem (14)] due to the average nature of the measurement of ψ^{leaf} and the need to disrupt the tissue to gain hydraulic access to the xylem (64).

Here, we used AquaDust to monitor in situ water-potential gradients in an intact, mature, transpiring maize leaf during the development of soil-moisture stress. Fig. 4*A* shows, schematically, the sites in which we infiltrated AquaDust into maize leaves for measurements of local ψ^{leaf} along the leaf. Fig. 4*B* shows the $\psi^{\mathrm{leaf}}_{\mathrm{AQD}}$ on node ($z = L/6$), mid ($z = L/2$), and tip ($z = 5L/6$) of the maize leaf. Under well-watered (WW) conditions, we observed a gradient ranging from 0.11 to 0.22 MPa/m from the node to the tip of the leaf, with an average transpiration rate of $E = 4.2 \times 10^{-5} \pm 0.85 \times 10^{-5}$ (range) $\mathrm{kg.m^{-2}.s^{-1}}$, but no significant difference was observed between the three positions of the leaf (see *SI Appendix*, section S5A and Table S5 for details). Similar values of transpiration-induced gradients have been reported for maize leaves, as measured by using an isopiestic psychrometer [gradient of 0.17 MPa/m, $E = 2.9 \times 10^{-5}$ $\mathrm{kg.m^{-2}.s^{-1}}$; (65)] and gradients predicted from the hydraulic architecture model for maize leaves [gradient of ∼0.1 MPa/m, $E = 2.6 \times 10^{-5}$ $\mathrm{kg.m^{-2}.s^{-1}}$; (66)]. Under water-limited

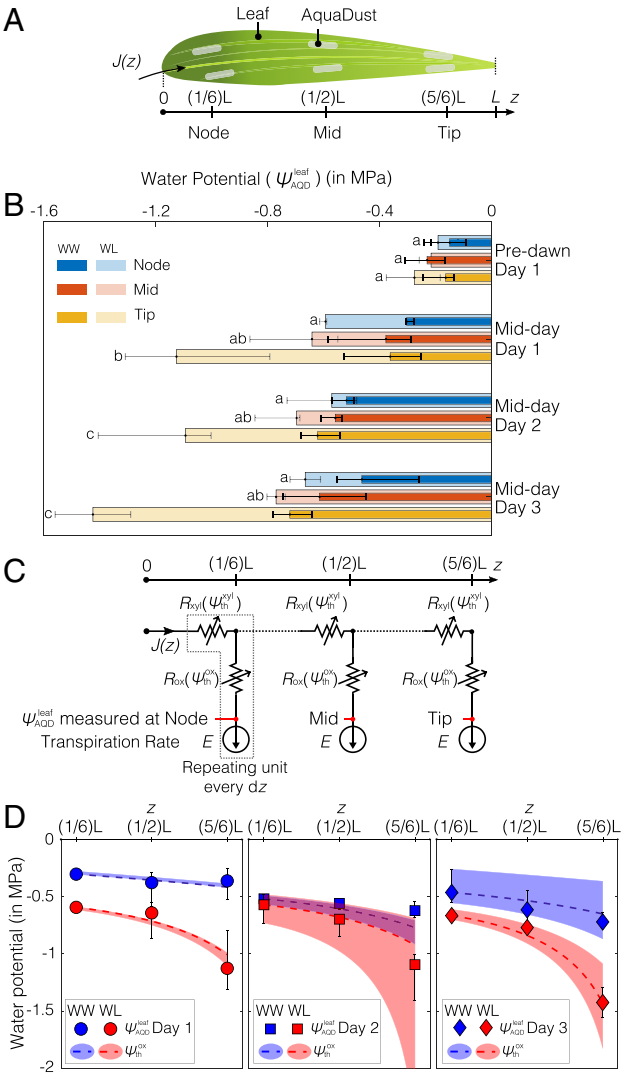

Fig. 4. Measurements of water potential gradients along a leaf. (*A*) Illustration of a maize leaf with AquaDust infiltrated at the node (first one-third of leaf blade connected to stem), mid (next one-third of leaf blade), and tip (final one-third of leaf blade). (*B*) Water potential measured using AquaDust ($\psi^{\mathrm{leaf}}_{\mathrm{AQD}}$) at node, mid, and tip of the leaf on maize plants in WW condition at predawn (∼ 0500 h) and midday (∼ 1400 h) for 3 d (days 1, 2, and 3); and for plants left unwatered (WL) for 1 d (day 1) at predawn (∼ 0500 h) and midday (∼ 1400 h); plants left unwatered for 2 d at midday (day 2); and plants left unwatered for 3 d at midday (day 3). Bar length and error bars represent the median and the full range, respectively, of water potential obtained using three measurements per AquaDust infiltration zone on three different plants. The a,b, ab, and c letters on the left side of each bar denote the Tukey's honestly significant difference test result of $\psi^{\mathrm{leaf}}_{\mathrm{AQD}}$ among leaf positions under the WL condition. Under WW treatment, $\psi^{\mathrm{leaf}}_{\mathrm{AQD}}$ were not significantly different among tip, mid, and node of the leaf (see *SI Appendix*, section S5A and Tables S5 and S6 for details). (*C*) Diagram of a hypothetical hydraulic circuit model of leaf with three segments (node, mid, and tip) that correspond to the sites of measurements in *B*. In each segment, the resistances both in the xylem (R_{xyl}) and outside the xylem (R_{ox}) depend on the local xylem and outside-xylem water potential ($\psi^{\mathrm{xyl}}_{\mathrm{th}}$ and $\psi^{\mathrm{ox}}_{\mathrm{th}}$). Transpiration rate ($E$) is constant and leads to a position-dependent flux in the xylem, $J(z)$. The measurements of water potential with AquaDust are assumed to correspond to $\psi^{\mathrm{ox}}_{\mathrm{th}}$ in each segment. (*D*) Predictions of $\psi^{\mathrm{ox}}_{\mathrm{th}}$ (dashed curves) with the model in *C* are compared against the water potential measured by using AquaDust ($\psi^{\mathrm{leaf}}_{\mathrm{AQD}}$) from WW and WL plants (from *B*) on 3 d with $E = 4.2 \times 10^{-5} \pm 0.85 \times 10^{-5}$ kg/(m^2.s) (range); the color-coded shaded regions represent the range of values based on the range of imposed rates of transpiration. (See *SI Appendix*, section S5C for details of the model.)

(WL) conditions, we observed significantly ($P < 0.05$) larger gradients between three positions of the leaf at midday on days 1, 2, and 3, in particular, between the midpoint and the tip of the leaves, with an average gradient of 0.7 MPa/m from the node to the tip of the leaf (see *SI Appendix*, section S5A and Table S6 for details). This large increase in the gradient relative to the WW case suggests a substantial loss of conductance with increasing stress. Indeed, the significant ($P < 0.05$) potential drop from node to tip for a plant with limited water supply (WL) for days 2 and 3 was threefold larger than that from the node to the tip in a WW plant (Fig. 4*B*). In addition, we found highly significant difference ($P < 0.01$) in ψ^{leaf} between the WW and WL treatments (see *SI Appendix*, section S5A and Table S7 for details).

In analyzing the trends observed in Fig. 4*B* for WW and WL gradients, we can take advantage of the localization of AquaDust in the mesophyll, outside the xylem at the terminal end of the hydraulic pathway (Fig. 2*C*). This localization allows us to test hydraulic models of the intact leaf with explicit hypotheses about the partitioning of resistance between the xylem and outside-xylem components of the pathway. We first tested a hypothesis in which xylem presents the limiting resistance to water flow (*SI Appendix*, section S5B and Fig. S17). Starting with the magnitude and ψ dependence ("vulnerability") of xylem resistance ($R_{\mathrm{xyl}}(\psi_{\mathrm{xyl}})$) reported by Li et al. (67), we could not predict the variations measured with AquaDust (Fig. 4*B*), even with extreme adjustments of parameter values (*SI Appendix*, Fig. S17). Secondly, we investigated the model represented in Fig. 4*C* in which both the resistances of the xylem (R_{xyl}) and those outside the xylem (R_{ox}) sit upstream of the location of our measurements with AquaDust based on the distribution that we observed in Fig. 2 (also see *SI Appendix*, Fig. S6).

Fig. 4*C* presents a hypothetical hydraulic circuit model of the leaf with three segments that match our measurements at node, midleaf, and tip. We note that this hydraulic circuit model does not require explicit values of soil water potential. In each segment, the xylem resistance (R_{xyl}) and outside-xylem resistance (R_{ox}) depend on the local values of water potential (ψ^{xyl} and ψ^{ox}, respectively). We used logistic functions to represent these "vulnerability curves," $R_{\mathrm{xyl}}(\psi^{\mathrm{xyl}})$ and $R_{\mathrm{ox}}(\psi^{\mathrm{ox}})$. These logistic functions are parameterized by the WW values of resistance ($R(\psi = 0)$) and the potential at 50% loss of conductance (or doubling of resistance—$\psi_{50\%}$). For R_{xyl}, we adopted parameter values from the literature (66, 67): $R_{\mathrm{xyl}}(\psi = 0) = 3.47 \times 10^3\ \mathrm{m^2.s.MPa/kg}$ and $\psi^{\mathrm{xyl}}_{50\%} = -1.58\ \mathrm{MPa}$. We did not find appropriate values in the literature for $R_{\mathrm{ox}}(\psi_{\mathrm{ox}})$ in maize.

We used this model to make predictions of ψ^{xyl} and ψ^{ox} at each segment for uniform, steady-state transpiration, $E = 4.2 \times 10^{-5} \pm 0.85 \times 10^{-5}\ \mathrm{kg.m^{-2}.s^{-1}}$ based on our gas-exchange measurements (see *SI Appendix*, section S5A for details). We compared the predicted values of ψ_{ox} to those for measured with AquaDust, $\psi^{\mathrm{leaf}}_{\mathrm{AQD}}$. As described in detail in *SI Appendix* (section S5C and Fig. S18), we optimized the parameters in $R_{\mathrm{ox}}(\psi_{\mathrm{ox}})$ to fit our measurements across both WW and WL conditions and all days; we obtained $R_{\mathrm{ox}}(\psi = 0) = 3.7 \times 10^3\ \mathrm{m^2.s.MPa/kg}$ and $\psi^{\mathrm{ox}}_{50\%} = -0.45$ MPa corresponding to mean *ET*. We found that this model (Fig. 4*C*) is consistent within the uncertainty in transpiration rate (shaded regions in Fig. 4*D*) with all measurements of local stress. Further, our optimal parameter values of ψ-dependence for extravascular resistance were in the range reported for the mesophyll resistance obtained for different species based on the vacuum-pressure method and modeling studies (58, 59).

The agreement between $\psi^{\mathrm{leaf}}_{\mathrm{AQD}}$ and $\psi^{\mathrm{ox}}_{\mathrm{th}}$ supports existing assessments of leaf hydraulics with respect to the dominance of extravascular resistance. The agreement between $\psi^{\mathrm{leaf}}_{\mathrm{AQD}}$ and $\psi^{\mathrm{ox}}_{\mathrm{th}}$ also reinforces our interpretation, based on the localization of AquaDust (Fig. 2*C*), that it measures outside-xylem water potential. Our observations demonstrate the capability of AquaDust to serve as an in situ reporter of local ψ and to help better understand the partitioning and responsiveness of resistances in leaves.

Documentation of Diurnal Variation in Leaf Water Potential in Intact Plants in the Field. The relative rates of water loss (transpiration) and water uptake control the water status of a plant. Evaporative demand varies with net radiation, relative humidity, air temperature, wind speed, and soil water status, as well as physiological responses of the plant, resulting in fluctuations in ψ^{leaf} (Fig. 1*A*). To date, access to the dynamics of plant water stress in the field has required destructive sampling of tissues (e.g., one leaf per measurement with pressure chamber) or inference from measurements in the soil and atmosphere (eddy covariance, etc.). It is also worth noting that inference on water status from the eddy-covariance method is complex, and modeling requires years of effort in calibrating transpiration and canopy conductance with respect to plant water status. One of the advantages of AquaDust is that it provides minimally invasive measurements of intact plant tissues and, hence, can be used for repeated measurements of water status on individual leaves to track dynamics. The response time of the AquaDust to a step change in water potential occurs on the order of seconds (*SI Appendix*, section S4O and Fig. S15). The response time of leaves to the changes in environmental conditions is expected to be on the order of 15 min (68); hence, AquaDust opens opportunities to study water-stress response of leaves to changing external environmental conditions. Here, we used AquaDust to measure the diurnal variation in leaf water potential and compared the predicted leaf water potential based on a soil–plant–atmosphere hydraulic resistance model informed by the model in Fig. 4 *C* and *D* with the measured $\psi^{\mathrm{leaf}}_{\mathrm{AQD}}$ over the course of a day in field conditions.

We found general agreement between calibration of AquaDust in growth chamber and the calibration of AquaDust in field conditions (see *SI Appendix*, section S4P and Fig. S16 for details). We note, though, that the correspondence between AquaDust response and pressure-chamber measurements was not as robust in the field as in the greenhouse and growth chamber; as discussed in *SI Appendix*, section S4P, we interpret the discrepancies observed as being due to heterogeneity in the microenvironment experienced by leaves in the field during our measurements. Once calibrated, we documented changes in $\psi^{\mathrm{leaf}}_{\mathrm{AQD}}$ of maize leaves over a period of 15 h in a well-irrigated field (minimal effect of soil moisture status). We performed measurements on two adjacent maize plants in an instrumented research plot at Cornell's Musgrave Research Farm (location: 42°43′N, 76°39′W). With AquaDust infiltration in leaves 4 and 7, we acquired three measurements per leaf once or more per hour throughout the day (except during field irrigation between 0800 and 1100 EST; Fig. 5*B*). We compared $\psi^{\mathrm{leaf}}_{\mathrm{AQD}}$ with the prediction of $\psi^{\mathrm{xyl}}_{\mathrm{th}}$ and $\psi^{\mathrm{ox}}_{\mathrm{th}}$ obtained by using a hydraulic resistance model with the resistance from a maize leaf, as shown in Fig. 4*C* [see *SI Appendix*, section S5D and Fig. S19 for details (69–71)] with the following inputs: 1) We used eddy covariance to estimate rates of transpiration (E; Fig. 5*A*); 2) we used the values of xylem resistance ($R_{\mathrm{xyl}}(\psi^{\mathrm{xyl}}_{\mathrm{th}})$) and outside-xylem resistance ($R_{\mathrm{ox}}(\psi^{\mathrm{ox}}_{\mathrm{th}})$) inferred from the observed gradient of water potential along the leaf in the previous section (*Water Potential Gradients along the Leaf* and Fig. 4); and 3) we assumed that soil was saturated ($\psi^{\mathrm{soil}} = 0$), and root and stem presented negligible resistance to water uptake under WW field conditions. The measurements of the diurnal dynamics of $\psi^{\mathrm{leaf}}_{\mathrm{AQD}}$ agreed favorably with the predictions

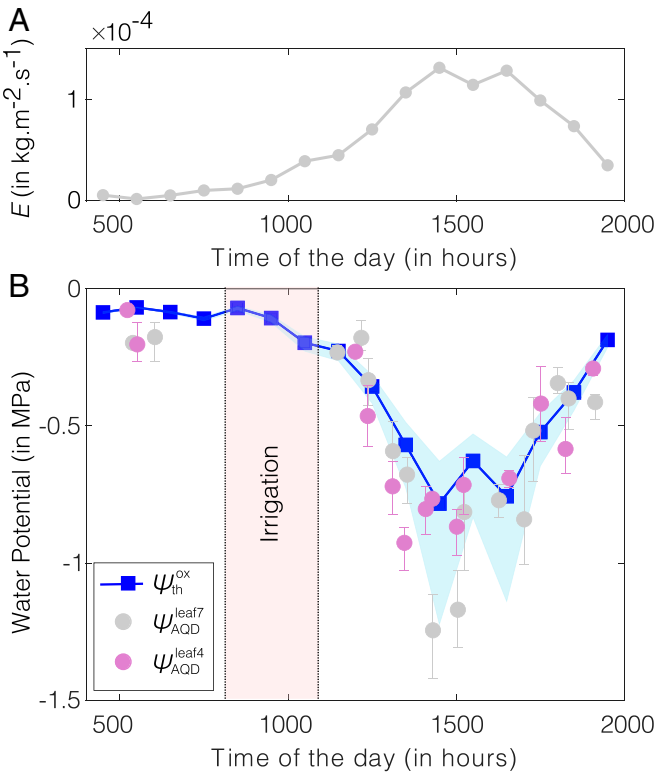

Fig. 5. In-field diurnal measurements of leaf water potential using AquaDust. (*A*) Hourly averaged transpiration (*E*) measured by using the eddy covariance method. (*B*) Values of water potential at tips of leaves 4 and leaves 7 measured with AquaDust (ψ_{AQD}^{leaf4}, ψ_{AQD}^{leaf7}) compared with the predicted diurnal variation of outside-xylem water potential (ψ_{th}^{ox}) obtained by using soil–plant–atmosphere hydraulic resistance model defined based on model and data in Fig. 4 *C* and *D* (see *SI Appendix*, section S5D and Fig. S19 for details on the model). Error bars represent the range of water potential from two biological replicates (plants) with three measurements per replicate. The shaded blue region represents the range on theoretical prediction of ψ_{th}^{ox} corresponding to the minimum and maximum value of outside-xylem resistance inferred from water potential gradients (shown in Fig. 4*C*; see *SI Appendix*, Fig. S18 for the numerical values of resistances).

of the model, further validating the model for the maize leaf (Fig. 4*C*) and limiting resistance for water loss being located in tissue outside the xylem. We compared the prediction from this model with the diurnal leaf water potential of lower-, middle-, and upper-canopy leaves measured using the pressure chamber in the field (see *SI Appendix*, section S5E and Fig. S20 for details). Pressure-chamber measurements performed in the middle and upper canopy agreed within uncertainty with the predictions of the model; measurements at the lower canopy remained near predawn potential, suggesting weak transpiration from these leaves (see *SI Appendix*, section S5E and Fig. S20 for details). This agreement again supports the appropriateness of our model. We also acknowledge that this model makes simplifying assumptions with respect to uniform xylem and outside-xylem vulnerability throughout the leaf and spatially uniform ET; more research is needed to gain further insight into the validity of these assumptions. This work demonstrates the potential for AquaDust to track plant water status under variable climate conditions with minimal perturbation, allow for rapid and repeated measures of ψ^{leaf}, and aid in more realistic modeling aimed at understanding local-scale water transport in leaves.

Conclusion

Our approach, based on hydrogel-based nanosensors, AquaDust, allows for in situ, minimally invasive measurements of water potential in local physiologically relevant microenvironments. This tool opens opportunities for better understanding of physics and biology of water dynamics in plants. As the process of AquaDust infiltration in leaves and fluorescence readout matures, AquaDust could be used for a high-throughput phenotyping strategy that allows for the discovery and quantification of new traits impacting water-use efficiency in crops. AquaDust, given its scale and localization within the mesophyll, provides opportunities to map gradients of water potential driving water flux from xylem to mesophyll and to atmosphere and to identify the major resistances along the pathway from node to the sites of evaporation. It also opens up possibilities to address key questions that center on providing an independent estimate of the water potential of the evaporative surfaces during transpiration, critical in measurements of exchange of carbon dioxide and water vapor (56, 72). As a tool for optical mapping of water potential, AquaDust has the potential to serve in a variety of contexts beyond leaves: in the rhizosphere, the critical root-associated volumes of soil in which water dynamics remains poorly characterized (73); in biophysical studies across species, in which responses to local water availability are of interest (74); and in nonbiological contexts—food science, geo-technical engineering, and material synthesis—in which the thermodynamics and transport of water are important (75–77).

Materials and Methods

Materials and methods for synthesis, characterization, calibration, and usage of AquaDust are described in *SI Appendix*.

Data Availability. All study data are included in the article and/or supporting information.

ACKNOWLEDGMENTS. We thank Glenn Swan and Nicholas S. Kaczmar for technical assistance; Prof. William Philpot for providing ST2000 spectrometer and optical fiber probes; Prof. Jocelyn K. C. Rose and Dr. Iben Sorensen for their technical support for sample preparation for the confocal imaging; Dr. Olivier Vincent for assistance in using vacuum setup; and Jacob L. Wszolek (Cornell Guterman Laboratory) for maintaining the plants in greenhouse and growth chamber. This work was supported by US Department of Agriculture National Institute of Food and Agriculture Agriculture and Food Research Initiative Competitive Grant 2017-67007-25950; and Air Force Office of Scientific Research Grant FA9550-18-1-0345. This work was also supported by Next-Generation BioGreen 21 Program Project PJ01321305, Rural Development Administration, Republic of Korea. This work was performed in part at the Cornell University Biotechnology Resource Center (NIH Grant S10RR025502 for data collected on the Zeiss LSM 710 Confocal and NIH Grant S10OD018516 for data collected on the upright Zeiss LSM880 confocal microscope [u880]) and in part at the Cornell NanoScale Facility, a member of the National Nanotechnology Infrastructure Network (NSF Grant NNCI-2025233).

1. Food and Agriculture Organization of the United Nations, "Water for sustainable food and agriculture" (Tech. Rep., Food and Agriculture Organization of the United Nations, Rome, Italy, 2017).
2. A. D. Stroock, V. V. Pagay, M. A. Zwieniecki, N. M. Holbrook, The physicochemical hydrodynamics of vascular plants. *Annu. Rev. Fluid Mech.* **46**, 615–642 (2013).
3. E. D. Schulze, Carbon dioxide and water vapor exchange in response to drought in the atmosphere and in the soil. *Annu. Rev. Plant Physiol.* **37**, 247–274 (1986).
4. K. Shackel, A plant-based approach to deficit irrigation in trees and vines. *Hortscience* **46**, 173–177 (2011).
5. H. McCutchan, K. A. Shackel, Stem-water potential as a sensitive indicator of water stress in prune trees (*Prunus domestica* L. Cv. French). *J. Am. Soc. Hortic. Sci.* **117**, 607–611 (1992).
6. N. C. Turner, Techniques and experimental approaches for the measurement of plant water status. *Plant Soil* 58, 339–366 (1981).
7. P. S. Nobel, *Physicochemical and Environmental Plant Physiology* (Academic Press, New York, NY. ed. 2, 1999).
8. B. Choat *et al.*, Global convergence in the vulnerability of forests to drought. *Nature* **491**, 752–755 (2012).

9. S. D. Wullschleger, M. A. Dixon, D. M. Oosterhuis, Field measurement of leaf water potential with a temperature-corrected in situ thermocouple psychrometer. *Plant Cell Environ.* **11**, 199–203 (1988).
10. M. A. Dixon, M. T. Tyree. A new stem hygrometer, corrected for temperature gradients and calibrated against the pressure bomb. *Plant Cell Environ.* **7**, 693–697, 1984.
11. P. F. Scholander, H. T. Hammel, E. D. Bradstreet, E. A. Hemmingsen, Sap pressure in vascular plants: Negative hydrostatic pressure can be measured in plants. *Science* **148**, 339–346 (1965).
12. E. M. Martinez, J. J. Cancela, T. S. Cuesta, X. X. Neira, Review. Use of psychrometers in field measurements of plant material: Accuracy and handling difficulties. *Spanish J. Agric. Res.* **9**, 313 (2011).
13. P. J. Kramer, J. S. Boyer, *Water Relations of Plants and Soils* (Academic Press, New York, NY, 1995).
14. L. Sack, N. M. Holbrook, Leaf hydraulics, *Annu. Rev. Plant Biol.* **57**, 361–381 (2006).
15. F. E. Rockwell, N. M. Holbrook, A. D. Stroock, Leaf hydraulics I: Scaling transport properties from single cells to tissues. *J. Theor. Biol.* **340**, 251–266 (2014).
16. T. N. Buckley, G. P. John, C. Scoffoni, L. Sack, The sites of evaporation within leaves. *Plant Physiol.* **173**, 1763–1782 (2017).
17. T. Okano, Y. H. Bae, H. Jacobs, S. W. Kim, Thermally on-off switching polymers for drug permeation and release. *J. Contr. Release* **11**, 255–265 (1990).
18. D. E. Owens *et al.*, Thermally responsive swelling properties of polyacrylamide/poly(acrylic acid) interpenetrating polymer network nanoparticles. *Macromolecules* **40**, 7306–7310 (2007).
19. P. J. Flory, J. Rehner, Statistical mechanics of cross-linked polymer networks I. Rubberlike elasticity. *J. Chem. Phys.* **11**, 512–520 (1943).
20. P. J. Flory, *Principles of Polymer Chemistry* (Cornell University Press, Ithaca, NY, 1953).
21. P. J. Flory, J. Rehner, Statistical mechanics of cross-linked polymer networks II. Swelling. *J. Chem. Phys.* **11**, 521–526 (1943).
22. T. Tanaka, Collapse of gels and the critical endpoint. *Phys. Rev. Lett.* **40**, 820–823 (1978).
23. V. F. Janas, F. Rodriguez, C. Cohen, Aging and thermodynamics of polyacrylamide gels. *Macromolecules* **13**, 977–983 (1980).
24. D. Nicoli, C. Young, T. Tanaka, A. Pollak, G. Whitesides, Chemical modification of acrylamide gels: Verification of the role of ionization in phase transitions. *Macromolecules* **16**, 887–890 (1983).
25. H. R. Maurer, *Disc Electrophoresis and Related Techniques of Polyacrylamide Gel Electrophoresis*, K. Fischbeck, Ed. (Walter de Gruyter & Co., Berlin, 1971).
26. A. K. Denisin, B. L. Pruitt, Tuning the range of polyacrylamide gel stiffness for mechanobiology applications. *ACS Appl. Mater. Interfaces* **8**, 21893–21902 (2016).
27. J. Baselga, I. Hernández-Fuentes, R. M. Masegosa, M. A. Llorente, Effect of crosslinker on swelling and thermodynamic properties of polyacrylamide gels. *Polym. J.* **21**, 467–474 (1989).
28. M. Ilavský, Phase transition in swollen gels. 2. Effect of charge concentration on the collapse and mechanical behavior of polyacrylamide networks. *Macromolecules* **15**, 782–788 (1982).
29. K. J. Dietz, S. Herth, Plant nanotoxicology. *Trends Plant Sci.* **16**, 582–589 (2011).
30. M. Antonietti, R. Basten, S. Lohmann, Polymerization in microemulsions—a new approach to ultrafine, highly functionalized polymer dispersions. *Macromol. Chem. Phys.* **196**, 441–466 (1995).
31. Y. S. Leong, F. Candau, Inverse microemulsion polymerization. *J. Phys. Chem.* **86**, 2269–2271 (1982).
32. H. A. Clark, M. Hoyer, M. A. Philbert, R. Kopelman, Optical nanosensors for chemical analysis inside single living cells. 1. Fabrication, characterization, and methods for intracellular delivery of PEBBLE sensors. *Anal. Chem.* **71**, 4831–4836 (1999).
33. H. A. Clark, R. Kopelman, R. Tjalkens, M. A. Philbert, Optical nanosensors for chemical analysis inside single living cells. 2. Sensors for pH and calcium and the intracellular application of PEBBLE sensors. *Anal. Chem.* **71**, 4837–4843 (1999).
34. N. Munshi, T. K. De, A. Maitra, Size modulation of polymeric nanoparticles under controlled dynamics of microemulsion droplets. *J. Colloid Interface Sci.* **190**, 387–91 (1997).
35. H. Campos, M. Cooper, J. E. Habben, G. O. Edmeades, J. R. Schussler, Improving drought tolerance in maize: A view from industry. *Field Crop. Res.* **90**, 19–34 (2004).
36. R. Huang, C. J. Birch, D. L. George, "Water use efficiency in maize production—the challenge and improvement strategies" in *Proceeding of 6th Triennial Conference*, E. Humphreys, Ed. (Maize Association of Australia, 2006), pp. 1–7.
37. T. Reeves, G. Thomas, G. Ramsay, *Save and Grow in Practice: Maize, Rice, Wheat* (Food and Agriculture Organization of the United Nations, Rome, Italy, 2016).
38. T. Nelson, J. A. Langdale, Patterns of leaf development in C4 plants. *Plant Cell* **1**, 3–13 (1989).
39. J. A. Langdale, B. Lane, M. Freeling, T. Nelson, Cell lineage analysis of maize bundle sheath and mesophyll cells. *Dev. Biol.* **133**, 128–139 (1989).
40. E. Acevedo, F. Elias, T. C. Hsiao, D. W. Henderson, Diurnal growth trends, water potential, and osmotic adjustment of maize and sorghum leaves in the field. *Plant Physiol.* **64**, 476–480 (1979).
41. A. Diaspro, *Nanoscopy and Multidimensional Optical Fluorescence Microscopy* (CRC Press, Boca Raton, 2010).
42. G. Bunt, F. S. Wouters, FRET from single to multiplexed signaling events. *Biophys. Rev.* **9**, 119–129 (2017).
43. E. A. Jares-Erijman, T. M. Jovin, FRET imaging. *Nat. Biotechnol.* **21**, 1387–1395 (2003).
44. A. Aneja, N. Mathur, P. K. Bhatnagar, P. C. Mathur, Triple-FRET technique for energy transfer between conjugated polymer and TAMRA dye with possible applications in medical diagnostics. *J. Biol. Phys.* **34**, 487–493 (2008).
45. I. Medintz, N. Hildebrandt, *FRET—Förster Resonance Energy Transfer: From Theory to Applications* (Wiley, Weinheim, Germany, 2013).
46. P. Bastiaens *et al.*, Resonance energy transfer from a cylindrical distribution of donors to a plane of acceptors. *Biophys. J.* **58**, 665–675 (1990).
47. P. K. Wolber, B. S. Hudson, An analytic solution to the Förster energy transfer problem in two dimensions. *Biophys. J.* **28**, 197–210 (1979).
48. S. Pelet, M. J. R. Previte, P. T. C. So, Comparing the quantification of Förster resonance energy transfer measurement accuracies based on intensity, spectral, and lifetime imaging. *J. Biomed. Opt.* **11**, 034017 (2006).
49. N. C. Turner, Stomatal behavior and water status of maize, sorghum, and tobacco under field conditions. *Plant Physiol.* **53**, 360–365 (1974).
50. O. Vincent, B. Marguet, A. D. Stroock, Imbibition triggered by capillary condensation in nanopores. *Langmuir* **33**, 1655–1661 (2017).
51. A. Martinière *et al.*, Uncovering pH at both sides of the root plasma membrane interface using noninvasive imaging. *Proc. Natl. Acad. Sci. U.S.A.* **115**, 6488–6493 (2018).
52. Q. Zhao, J. Sun, Y. Lin, Q. Zhou, Study of the properties of hydrolyzed polyacrylamide hydrogels with various pore structures and rapid pH-sensitivities. *React. Funct. Polym.* **70**, 602–609 (2010).
53. H. Sun, K. Almdal, T. L. Andresen, Expanding the dynamic measurement range for polymeric nanoparticle pH sensors. *Chem. Commun.* **47**, 5268–5270 (2011).
54. I. D.. Johnson, "Fluorescein, Oregon green and rhodamine green dyes—section 1.5" in *Molecular Probes Handbook: A Guide to Fluorescent Probes and Labeling Technologies* (Life Technologies Corporation, Carlsbad, CA, ed. 11, 2010), pp. 66–73.
55. T. J. Brodribb, S. A. M. McAdam, Evolution of the stomatal regulation of plant water content. *Plant Physiol.* **174**, 639–649 (2017).
56. L. A. Cernusak *et al.*, Unsaturation of vapour pressure inside leaves of two conifer species. *Sci. Rep.* **8**, 1–7 (2018).
57. L. Sack, P. J. Melcher, M. A. Zwieniecki, N. M. Holbrook, The hydraulic conductance of the angiosperm leaf lamina: A comparison of three measurement methods. *J. Exp. Bot.* **53**, 2177–2184 (2002).
58. C. Scoffoni *et al.*, Outside-xylem vulnerability, not xylem embolism, controls leaf hydraulic decline during dehydration. *Plant Physiol.* **173**, 1197–1210 (2017).
59. P. Trifiló *et al.*, The contribution of vascular and extra-vascular water pathways to drought-induced decline of leaf hydraulic conductance. *J. Exp. Bot.* **67**, 5029–5039 (2016).
60. D. Xiong, J. Flexas, T. Yu, S. Peng, J. Huang, Leaf anatomy mediates coordination of leaf hydraulic conductance and mesophyll conductance to CO_2 in *Oryza*. *New Phytol.* **213**, 572–583 (2017).
61. S. Salleo, F. Raimondo, P. Trifilò, A. Nardini, Axial-to-radial water permeability of leaf major veins: A possible determinant of the impact of vein embolism on leaf hydraulics? *Plant Cell Environ.* **26**, 1749–1758 (2003).
62. U. Hochberg *et al.*, Stomatal closure, basal leaf embolism, and shedding protect the hydraulic integrity of grape stems. *Plant Physiol.* **174**, 764–775 (2017).
63. Y. J. Zhang, F. E. Rockwell, A. C. Graham, T. Alexander, N. M. Holbrook, Reversible leaf xylem collapse: A potential "circuit breaker" against cavitation. *Plant Physiol.* **172**, 2261–2274 (2016).
64. H. Cochard *et al.*, Methods for measuring plant vulnerability to cavitation: A critical review. *J. Exp. Bot.* **64**, 4779–4791 (2013).
65. A. C. Tang, J. S. Boyer, Growth-induced water potentials and the growth of maize leaves. *J. Exp. Bot.* **53**, 489–503 (2002).
66. W. Chunfang, M. T. Tyree, E. Steudle, Direct measurement of xylem pressure in leaves of intact maize plants. A test of the cohesion-tension theory taking hydraulic architecture into consideration. *Plant Physiol.* **121**, 1191–1205 (1999).
67. Y. Li, J. S. Sperry, M. Shao, Hydraulic conductance and vulnerability to cavitation in corn (*Zea mays* L.) hybrids of differing drought resistance. *Front. Plant Sci.* **66**, 341–346 (2009).
68. K. Raschke, Leaf hydraulic system: Rapid epidermal and stomatal responses to changes in water supply. *Science* **167**, 189–191 (1970).
69. S. Zhu, "Development of sensing framework for the soil-plant atmosphere continuum," PhD thesis, Cornell University, Ithaca, NY (2020).
70. G. L. Hammer *et al.*, Can changes in canopy and/or root system architecture explain historical maize yield trends in the U.S. corn belt?. *Crop Sci.* **49**, 299–312 (2009).
71. J. Zhuang, K. Nakayama, G. R. Yu, T. Urushisaki, Estimation of root water uptake of maize: An ecophysiological perspective. *Field Crop. Res.* **69**, 201–213 (2001).
72. T. N. Buckley, L. Sack, The humidity inside leaves and why you should care: Implications of unsaturation of leaf intercellular airspaces. *Am. J. Bot.* **106**, 618–621 (2019).
73. A. G. Bengough, Water dynamics of the root zone: Rhizosphere biophysics and its control on soil hydrology. *Vadose Zone J.* **11**, vzj2011.0111 (2012).
74. H. Tichy, E. Gingl, "Problems in hygro- and thermoreception" in *Ecology of Sensing*, F. G. Barth, A. Schmid, Eds. (Springer, Berlin, Germany, 2001), pp. 271–287.
75. J. A. Troller, *Water Activity and Food* (Academic Press, New York, NY, 1978).
76. S. R. Evett, G. W. Parkin, Advances in soil water content sensing: The continuing maturation of technology and theory. *Vadose Zone J.* **4**, 986–991 (2005).
77. C. J. Brinker, G. W. Scherer, *Sol-Gel Science: The Physics and Chemistry of Sol-Gel Processing* (Academic Press, Boston, 2013).